Calcium/synaptotagmin-evoked compound fusion increases quantal size and synaptic strenghth

Liming He[1*], Lei Xue[1*], Jianhua Xu[1], Benjamin D. McNeil[1], Li Bai[1], Ernestina Melicoff[2], Roberto Adachi[2] and Ling-Gang Wu[1]

1. National Institute of Neurological Disorders and Stroke, 35 Convent Dr., Bldg 35, Rm. 2B-1012, Bethesda, Maryland 20892

2. Department of Pulmonary Medicine, The University of Texas M. D. Anderson Cancer Center, 2121 W. Holcombe Blvd., Box 1100, Houston, Texas 77030

Supplementary Information

I. The Model for vesicle exocytosis and endocytosis at synapses

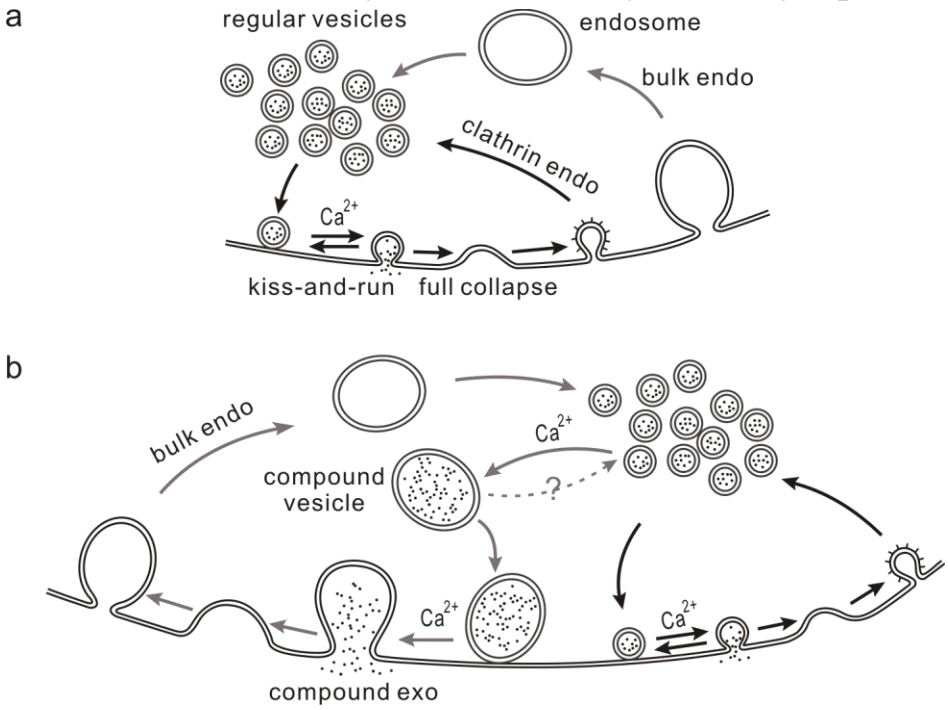

Figure S1. Modification of the current model on exocytosis and endocytosis at synapses

a, The current view.

b, Modification of the current view based on the present work. See text for explanation. Endo: endocytosis; kiss-and-run: kiss-and-run fusion and retrieval; Clathrin endo: clathrin-dependent endocytosis; exo: exocytosis.

Figure S1a shows the current view on the forms of vesicle fusion and endocytosis at synapses, where only vesicle fusion with the plasma membrane is considered[1,2]. After calcium-induced vesicle fusion with the plasma membrane, the fusion pore may close

rapidly at the same site of fusion (kiss-and-run form), or fully collapse with the plasma membrane, followed by clathrin-mediated endocytosis or bulk endocytosis (Fig. S1a).

The present work calls for modification of this current view, as illustrated in Fig. S1b. The modification includes 1) calcium-mediated compound fusion between vesicles to form large compound vesicles, 2) exocytosis of these compound vesicles (compound exocytosis) to increase quantal size, and 3) retrieval of fused compound vesicle membrane via bulk endocytosis to form large endosomes (Fig. S1b).

We assume that like endosomes, compound vesicles can also be converted to regular vesicles in a time scale of minutes. This may explain the slow recovery of the mEPSC size potentiation after tetanic stimulation (Fig. 4a, b, d). Since we do not have direct evidence supporting this assumption, we put a dash line and a question mark (?) in the transition from the compound vesicle to regular vesicles in Fig. S1b.

II. Issues about cell-attached recordings

1. Giant up-steps are not caused by multiple vesicle fusion at the plasma membrane

Considering that the mean up-step frequency was 0.16 Hz, the release probability in a 10 ms interval (this was longer than our time resolution) was 0.0016. If each vesicle fusion is independent, once we detect a vesicle fusion, the probability for an additional vesicle or more to fuse within the same 10 ms window is practically 0.0016 (probability = $0.0016 + 0.0016^2 + 0.0016^3 + \ldots$), which is much less than the percentage (20%) of giant up-steps being observed. Thus, most giant up-steps were not caused by independent fusion of multiple vesicles.

Coordinated release of only two vesicles from two different release sites has been proposed at ribbon-type synapses[3]. This hypothesis was not supported by any known mechanism that can coordinate multi-vesicular release between two release sites. In fact, compound fusion has been proposed to account for multiple vesicle fusion at ribbon-type synapses[4]. We do not think coordinated release underlies giant up-steps, because giant up-steps were ~3 – 40 times (mean = 571 aF or ~8 times) the mean vesicle size (73 aF)[5], whereas only ~2 vesicles are considered docked (within 10 nm from the plasma membrane) at each active zone[6]. Coordinating release of up to 40 vesicles from many active zones is therefore difficult to imagine, if not absolutely impossible. In addition, the calyx-type synapse contains conventional active zones, but not ribbons where coordinated release was proposed[6]. Our observation of the initial fusion pore (G_p, Fig. 1c) suggests that giant up-steps are due to fusion of a single membrane structure, which further argues against coordinated multi-vesicular release (for detail see the next paragraph). We concluded that a giant up-step corresponded to a single membrane structure larger than a single vesicle.

This paragraph lists the arguments based on G_p measurements suggesting that a giant up-step reflects fusion of a single membrane structure. In 6% of giant up-steps, we detected an initial G_p of 162 ± 41 pS (n = 10 up-steps, ranged from 44 to 370 pS, Fig. 1c). Assume that these giant up-steps were due to fusion of a number of identical vesicles, the number would be ~8, because the mean giant up-steps (571 aF) was ~8 times the mean regular up-step (73 aF)[5]. The G_p for each of these 8 identical vesicles would be ~20 pS (≈ 162/8). When these 8 vesicles were randomly selected from a large pool, the

probability of vesicles with a G_p of ~20 pS (or < 100 pS) should be 70.4% (= $0.06^{1/8}$) in order to match the 6% (= 0.704^8) chance of selecting all 8 vesicles with a G_p of ~20 pS. The measured mean G_p for regular up-steps was > 375 pS (Ref. [5]). A G_p < 100 pS was detected in ~1.4% of regular up-steps in a previous study[5]. When the sine wave frequency (20 kHz, if not mentioned) was increased to 90 kHz, which allowed for detecting a larger range of G_p values, a G_p of 256 ± 32 pS was detected in 10% of regular up-steps. Thus, the measured percentage (<10%) of regular up-steps with a G_p < 100 pS was much less than the percentage (70.4%) predicted under the assumption that giant up-steps were due to multi-vesicular fusion. We concluded that the assumption that giant up-steps were due to multi-vesicular fusion at the plasma membrane was incorrect.

2. Down-step amplitude distribution in control and during KCl application

The down-step amplitude distribution in control (Fig. S2a) and during KCl application (Fig. S2b) were used to generate the down-step amplitude cumulative probability plot in Fig. 1e of the main text.

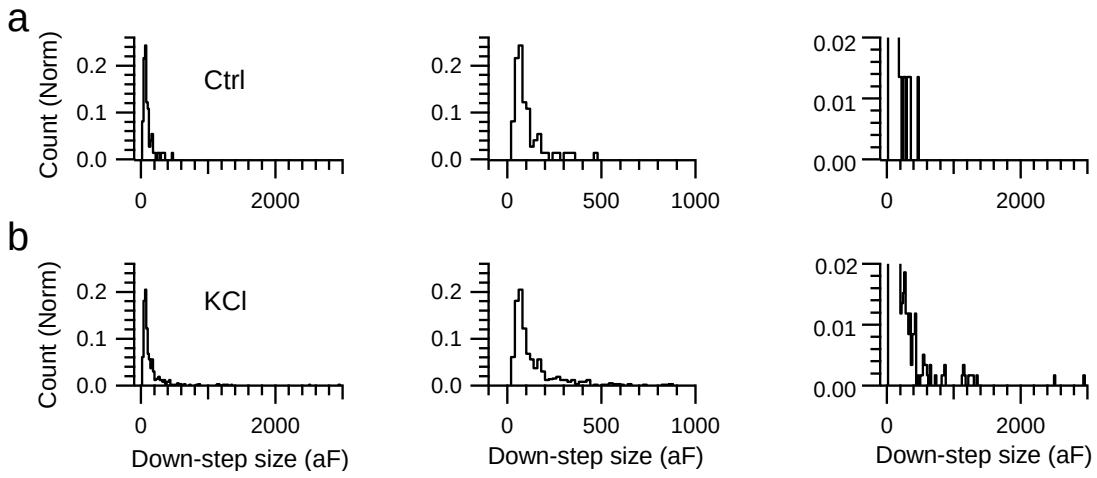

Figure S2. Down-step amplitude distribution

a, Left: Amplitude distribution of down-steps observed in control (74 down-steps from 78 patches). The number of down-steps was normalized to the total number (74 down-steps).
Middle: same as in left, but with the horizontal axis limited to < 1000 aF.
Right: same as in left, with the vertical axis limited to 0.02, indicating that a small fraction of down-steps were >220 aF.

b, Similar to panel a, but during high potassium application (591 down-steps from 17 patches).

3. The latency for the first regular up- and down-step during high KCl application

The first regular up-step was observed at 20 ± 2 s (n = 17 patches, Fig. S3) after KCl application, which was faster than that (47 ± 8 s, n = 17 patches, p < 0.01, Fig. 1g, h) of the first giant up-step. This may imply that giant up-steps were triggered by more prolonged calcium influx than regular up-steps.

The first regular down-step was observed at 56 ± 5 s (n = 17 patches, Fig. S3) after KCl application, which was slightly later than the first giant up-step (47 ± 8 s, n = 17 patches, p = 0.2). Thus, it was highly unlikely that the first giant up-step was caused by endocytosis of regular vesicles (regular down-steps), formation of large

endosome-like structures by these endocytosed regular vesicles, and re-exocytosis of the endosome-like structures, because such a cycle would take additional time to accomplish.

The first regular down-step (56 ± 5 s, n = 17 patches) was earlier than the first giant down-step (127 ± 26 s, n = 17 patches, $p < 0.01$). It was likely that bulk endocytosis took longer than regular vesicle endocytosis.

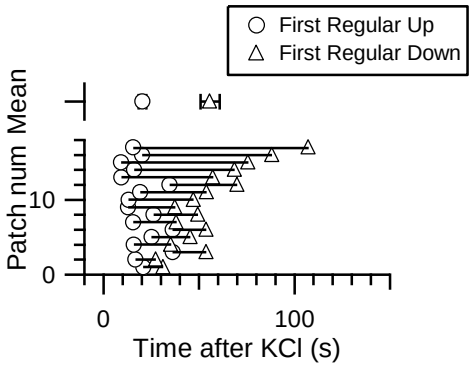

Figure S3. The latency for the first regular up- and down-step

The timing of the first regular up-step (circles) and the first regular down-step (triangles) after KCl application for each of 17 patches (lower). Their means are also plotted (upper).

III. Issues about mEPSC recordings

1. Release of larger vesicles generates larger mEPSCs with a slower rise time

The model synapse and parameters

We performed Monte Carlo simulations of quantal events at synapses with MCell 2.50[7] as described in detail in Ref. [5]. Briefly, the diffusion coefficient of glutamate was 3.3×10^{-6} cm^2/s (Ref. [8]). The pre- and postsynaptic sites of the synaptic cleft were modeled as planar sheets, 0.12 μm x 0.12 μm on each side, separated by a 20 nm cleft from the post-synaptic membrane (Fig. S4). A vesicle was aligned at the center of the presynaptic membrane sheet. The mean vesicle was modeled as a cube[9] with an inner edge length of 37 nm (Fig. S4). The volume of this cube is similar to a round vesicle with a diameter of 46 nm, the mean diameter of vesicles in the calyx[6]. The cube contained 10,000 glutamate molecules. Fifty AMPA receptors were arranged in a square with an area of 0.0144 μm^2 positioned at the center of the postsynaptic membrane sheet. This square was surrounded by annular-shaped pre- and postsynaptic barriers, each occupying 10% of the cleft width (2 nm). The reaction scheme for AMPA receptors was taken from Ref. [10]. Fusion occurred at the center of the presynatpic membrane sheet with a pore length of 15 nm, similar to the length of a gap junction[11]. Since the fusion pore opening is mostly too fast and/or too large to resolve[5], we assumed extremely rapid pore opening. In simulation, a rapid fusion pore conductance (G_p) increase at a rate of 5000 pS/ms was assumed. However, our conclusions held with various rates of G_p increase. Cleft glutamate was assessed as the average concentration in the volume of the cleft above the receptor field. The AMPA receptor scheme and other parameters commonly used for modeling synapses were chosen from our previous study[5].

Two vesicle sizes were chosen. The first one was the mean vesicle in the calyx with a diameter of 46 nm[6], and the second one was a vesicle with a diameter of 92 nm, which mimics a large vesicle caused by compound fusion between vesicles. The

equivalent inner edge length of the cube used for simulation would be 37nm and 74nm, respectively, for these two vesicles. Because the volume of the large vesicle was 8 times that of the mean vesicle, we assumed that the large vesicle contains 8 times of transmitter molecules as the mean vesicle. We assumed that the mean vesicle contains 10,000 glutamate molecules (see Ref. [5]). Thus, the large vesicle contains 80,000 glutamate molecules.

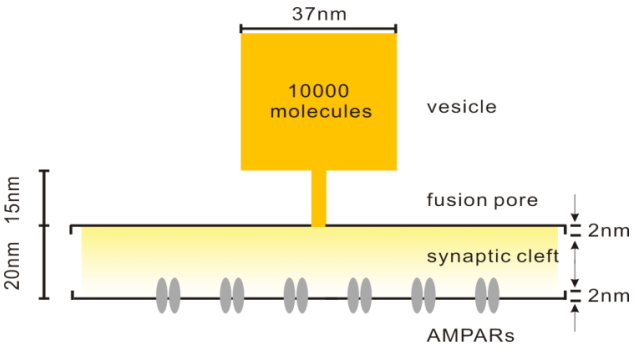

Figure S4. The model synapse for simulation.

The cube represents a vesicle with a diameter of 46 nm, the mean diameter of the vesicle in the calyx.

Results from simulation

We performed realistic simulation with MCell 2.50. For each vesicle size group, one hundred runs of a simulation were averaged. Results were plotted in Figure S5. The resulting peak number of the activated AMPA receptors (N_{AMPA_O}) is the mirror of the mEPSC current. The rise time of N_{AMPA_O} therefore represented the mEPSC rise time.

For the mean vesicle with a diameter of 46 nm, the peak of N_{AMPA_O} was ~17 (Fig. S5a), which was similar to the mean peak number (~22) of activated AMPA receptors experimentally estimated at the calyx-type synapse[12]. The 10-90% rise time of N_{AMPA_O} was 0.12 ms (Fig. S5a).

For the large vesicle with a diameter of 92 nm, the peak of N_{AMPA_O} was ~33 (Fig. S5), much larger than that (17) for the mean vesicle. The 10-90% rise time of N_{AMPA_O} was 0.17 ms (Fig. S5), much longer than that (0.12 ms) for the mean vesicle. These simulation results were consistent with our experimental result that mEPSCs > 80 pA had a 10-90% risetime (0.35 ms) longer than that (0.29 ± 0.01 ms, n = 10 cells) of mEPSCs < 80 pA (Fig. 3c).

The N_{AMPA_O} rise time (0.12 ms) was faster than the experimentally measured mEPSC rise time (0.306 ± 0.008 ms, n = 10 cells). As explained in detail in our previous study (Supplementary Information VII of Ref. [5]), the difference was largely due to low-pass filtering of the experimental data, recordings of mEPSCs without series resistance compensation (note: with series resistance compensation, the mean mEPSC rise time was ~0.21 ms), and an assumption that the fusion pore opening is nearly instantaneous. If we slowed the rate of G_p increase in simulation, the N_{AMPA_O} rise time would be slow (not shown). However, the principle that larger vesicles had a slower N_{AMPA_O} rise time held (not shown).

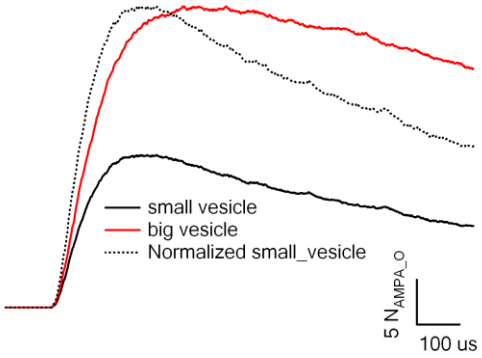

Figure S5. N_{AMPA_O} for small and large vesicles

The N_{AMPA_O} for a vesicle with a diameter of 46 nm (black) and for a vesicle with a diameter of 92 nm (red). The N_{AMPA_O} for a vesicle with a diameter of 46 nm was also scaled for comparison (dotted black)

2. The presynaptic origin of giant mEPSCs

To determine whether larger mEPSCs were due to higher glutamate concentrations in the synaptic cleft, we used γ-DGG, a competitive AMPA receptor blocker that blocks less effectively at higher glutamate concentrations. Before γ-DGG application, the mEPSCs during KCl application were obtained as control (Fig. S6a, black). After washout of KCl and bath application of γ-DGG (100 - 400 μM), mEPSCs were collected during another round of KCl application (Fig. S6a, red). Application of γ-DGG reduced the mEPSC amplitude during KCl application by 24 ± 2% (n = 9 synapses), and shifted the mEPSC amplitude cumulative probability curve to the left (Fig. S6a). This reduction was not due to rundown, because the mEPSC amplitude during the first and the second round of KCl application was similar (102 ± 2%, n = 5 cells) when γ-DGG was not added.

Next, we used a method described in Ref. [13] to determine whether γ-DGG had a smaller effect on large EPSCs. At any given cumulative probability level (Fig. S6a, Y), the corresponding mEPSC amplitude before (control, Fig. S6a, A_{Ctrl}) and after γ-DGG application (Fig. S6a, A_{DGG}) could be found. $R_{DGG/Ctrl}$, the ratio between A_{DGG} and A_{Ctrl} (see also Fig. S6b legend), increased as A_{Ctrl} increased in 8 out of 9 synapses (Fig. S6b, see legend for methods), suggesting that γ-DGG reduced larger mEPSCs by a smaller fraction. We did not measure $R_{DGG/Ctrl}$ when A_{Ctrl} was < 40 pA, because as A_{Ctrl} approached the threshold of detection (20 pA), a large error was introduced due to mEPSCs that were above the threshold of detection in control, but were reduced below the threshold by γ-DGG (for detail, see Ref. [13]).

As a control, bath application of NBQX (60 - 80 nM), which non-competitively blocks AMPA receptors to the same level regardless of the glutamate concentration, reduced the mEPSC amplitude by 26 ± 3% (n = 6, Fig. S6c). The ratio ($R_{NBQX/Ctrl}$) between the mEPSC amplitude in control (A_{Ctrl}) and that during NBQX application did not increase as A_{Ctrl} increased (Fig. S6d, n = 6 synapses). We concluded that large mEPSCs were due to higher glutamate concentrations in the synaptic cleft, consistent with release from larger vesicles.

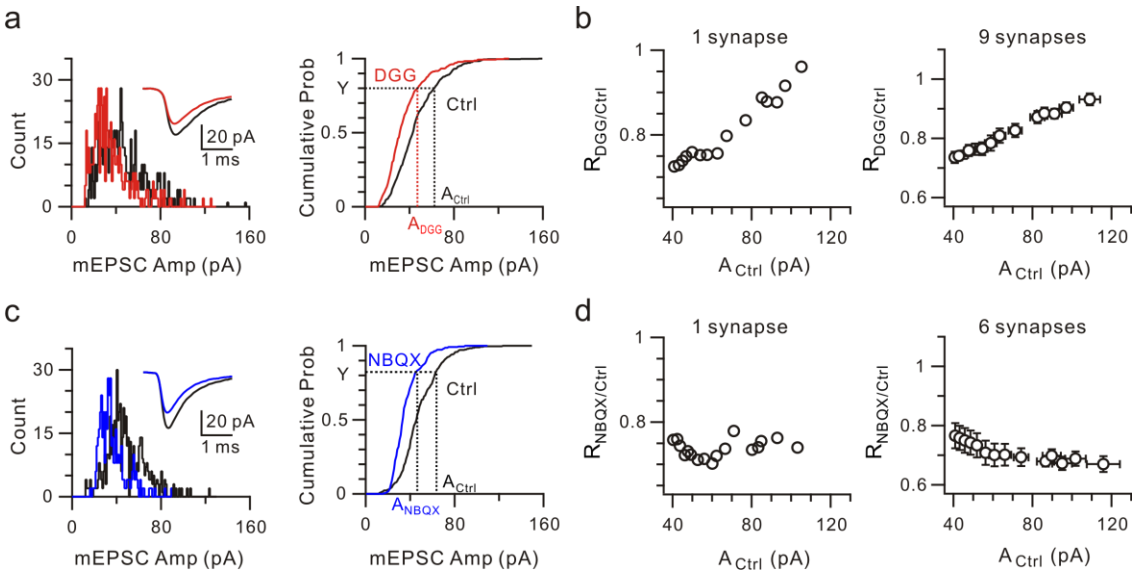

Figure S6. Large mEPSCs are caused by more transmitter release

a, The mEPSC amplitude distribution (left), and cumulative probability curve (right) obtained during KCl application in the absence (Ctrl, black) and the presence of γ-DGG (red, 300 μM). The inset in the left shows the mean mEPSC in the absence (n = 703 mEPSCs, black) and in the presence of γ-DGG (n = 624 mEPSCs, red). Dotted lines indicate that at a given cumulative probability level, Y, the corresponding mEPSC amplitude in control (A_{Ctrl}) and that after γ-DGG application (A_{DGG}) can be found. The ratio between A_{DGG} and A_{Ctrl} is $R_{DGG/Ctrl}$. Data were from 1 synapse.

b, Left: $R_{DGG/Ctrl}$, calculated from panel a (1 synapse), plotted versus A_{Ctrl}. Data with $A_{Ctrl} < 40$ pA were not included. $R_{DGG/Ctrl}$ was calculated for every 5% increase in the cumulative probability level and every 1% increase between 95 - 99% of the cumulative probability level.

Right: Similar to left, but pooled from 9 synapses. $R_{DGG/Ctrl}$ and the corresponding A_{Ctrl} from each cell were pooled, then sorted such that A_{Ctrl} ascended monotonically, and binned for every 6 - 9 values. The binned R values were plotted versus the corresponding binned A_{Ctrl} values.

c, Similar to a, except that γ-DGG is replaced with NBQX (60 nM, blue). The inset in the left shows the mean mEPSC in control (n = 586 mEPSCs, black) and in the presence of NBQX (n = 446 mEPSCs, blue). Data were from 1 synapse.

d, Similar to b, except that γ-DGG is replaced with NBQX (60 - 80 nM). Data in the left were taken from that shown in panel c. Data in the right were pooled from 6 synapses.

3. Does compound fusion saturates postsynaptic receptors?

In resting conditions, whole-cell dialysis of high concentrations of glutamate in the calyx increased the mEPSC amplitude by ~53%, indicating that the postsynaptic AMPA receptors are not saturated[13,14]. This gives room for the increase of the mEPSC amplitude during compound exocytosis. We found that high KCl application increased the up-step amplitude by ~103% (= 193/95 - 1), but the mEPSC by ~52% (=44.9/29.6 - 1). The discrepancy might be due to partial saturation of AMPA receptors by compound exocytosis of large vesicles and/or the difference in the recording techniques.

For the convenience of identifying compound fusion, we defined giant up-steps as up-steps more than 220 aF, the estimated membrane capacitance value of the largest

regular vesicles observed in resting condition. However, even if we measured up-steps only between 100 - 220 aF, the mean up-step amplitude during high potassium application (144 ± 2 aF, n = 291) was still significantly larger than that (133 ± 6 aF, n = 28) in control ($p < 0.05$). These results suggest that a significant amount of compound fusion may be due to fusion among 2 - 3 regular size (mean = 73 aF) vesicles during high potassium application. Compound fusion with a minimal number of vesicles may thus provide an economical way to increase the quantal size.

A small fraction (61 out of 857 up-steps, or 7%) of total up-steps was > 500 aF during KCl application, which may correspond to compound fusion among more than 6 - 7 mean size vesicles (73 - 84 aF)[5]. Release of such a giant vesicle may cause more saturation of postsynaptic receptors.

It should be noted that the postsynaptic response may not be necessarily proportional to the amount of transmitter in a vesicle. For example, in our simulation shown in Supplementary Information III-1, increasing the vesicle volume and thus the transmitter molecule number by 8 times (increasing the diameter by 2 times, from 46 nm to 92 nm) only increased the postsynaptic response by nearly 2 times (Fig. S5). Even with such an increase of the vesicle volume, the postsynaptic receptors were not fully saturated (33 out of 50 receptors are activated at the peak of N_{AMPA_O}, Fig. S5).

IV. Capacitance up- and down-steps reflect exo- and endocytosis

We have previously showed that up- and down-steps were blocked by dialysis of trypsin in the calyx, which blocks release but not calcium currents. Thus, up- and down-steps are not caused by calcium-dependent artifacts[5].

In the present work, we further determined whether giant up-steps occurred in mice lacking synaptotagmin II (Syt2), in which evoked release, but not calcium current was mostly blocked[15]. We found a low percentage (5%, 12 from 220 steps) of giant up-steps in resting conditions in *Syt2*$^{-/-}$ mice (Fig. 2e, f), which was similar to that (0%, 0 out of 26 up-steps) in *Syt2*$^{+/+}$ wild-type littermates. The percentage of giant up-steps was not increased by high KCl application in *Syt2*$^{-/-}$ mice (3.8%, χ^2 test, $p = 0.26$). In contrast, the percentage of giant up-steps was significantly increased by high KCl application in *Syt2*$^{+/+}$ wild-type littermates (Control: 0%, n =11 patches; KCl: 24% , n =11 patches; χ^2 test, $p < 0.05$). Thus, giant up-steps were mediated by Syt2, but not by KCl-induced depolarization alone, indicating that giant up-steps were not a result of KCl-induced artifacts.

More importantly, we found a strong correlation between the up-step and the mEPSC in both the frequency and the amplitude. The frequency of both up-steps and mEPSCs in resting conditions was ~20 - 40 times higher in *Syt2*$^{-/-}$ mice (up-step: 0.13 ± 0.04 Hz, n = 10; mEPSC: 13.9 ± 3.1 Hz, n = 9) than in wild-type littermates (up-step: 0.003 ± 0.001 Hz, n = 11; mEPSC: 0.7 ± 0.3 Hz, n = 6) (see also Ref. [15]). High KCl application increased both the up-step frequency (Ctrl: 0.13 ± 0.04 Hz, n = 10; KCl: 0.25 ± 0.08 Hz, n = 10) and the mEPSC frequency (Ctrl: 13.9 ± 3.1 Hz, n = 9; KCl: 18.8 ± 2.9 Hz, n = 9) by only less than 2 times in *Syt2*$^{-/-}$ mice, but increased both the up-step frequency (Ctrl: 0.003 ± 0.001 Hz, n = 11; KCl: 0.14 ± 0.02 Hz, n = 11) and the mEPSC frequency (Ctrl: 0.7 ± 0.3 Hz, n = 6; KCl: 7.8 ± 0.7 Hz, n = 6) by ~10 - 20 times in wild-type mice. High KCl application did not increase the up-step amplitude or the

mEPSC amplitude in *Syt2*$^{-/-}$ mice, but increased both of them significantly in wild-type *Syt2*$^{+/+}$ littermates (Figs. 2c-f, 3e-h). These results significantly strengthened our conclusion that up-steps, including giant ones, reflect fusion events.

In addition, we found that block of endocytosis by whole-cell dialysis of GDPβS into the same calyx, in which up-steps were recorded from a cell-attached patch, blocked down- but not up-step (Fig. 1h), confirming that down-steps reflect endocytosis.

V. Correlation between compound exocytosis and bulk endocytosis

Giant up-steps preceded giant down-steps during high KCl application (Fig. 1f, g). The mean percentages of both giant up- and down-steps were small in control (before KCl application, ~6% and ~8%), but increased to similar levels (20% and 17%) during high potassium application (Fig. S7a). The mean sizes of both giant up- and down-steps were small and similar in control (275 ± 22 aF vs 330 ± 31 aF), but increased to similar values (571 ± 36 aF vs 501 ± 42 aF) during high potassium application (Fig. S7b). The mean sizes of both up- and down-steps (including regular and giant) were small and similar in control (98 ± 12 aF, n = 7 patches vs 106 ± 16 aF, n = 7 patches), but increased significantly ($p<0.05$) to similar values (186 ± 19 aF, n = 17 patches vs 156 ± 12 aF, n = 17 patches) during high potassium application (Fig. S7c, see also the legend for why only 7 patches were used in control). These results suggest that the size of individual retrieval events depended on the size of individual fusion events. Giant up-steps were followed and coupled to giant down-steps for membrane recycling. Bulk endocytosis may retrieve vesicle membrane caused by compound exocytosis via a mechanism that maintains the identity of fused and retrieved vesicles or at least the area of them.

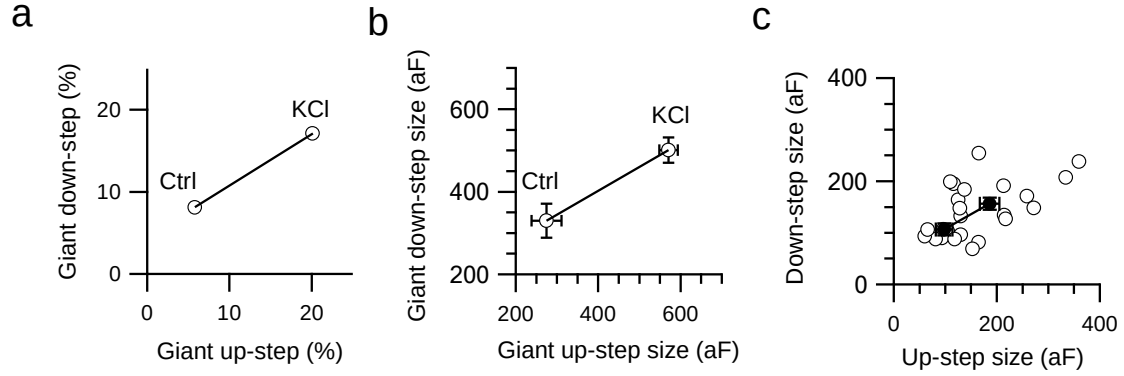

Figure S7. The correlation between down- and up-steps

a-b, The percentage (a) and the size (b) of giant down-steps (>220 aF) plotted versus those of giant up-step (>220 aF) obtained in control (Ctrl, n = 78 patches) and during high potassium application (KCl, n = 17 patches). Data are expressed as mean ± SE.

c, The mean size of down-steps (both regular and giant ones) plotted versus the mean size of up-step (both regular and giant ones) obtained from each patch in control (n = 7 patches) and during high potassium application (open circles, n = 17 patches). Two solid symbols are the mean (± SE) of all patches in control (lower) and that during high potassium application (upper). For patches in control, we only include those (7 patches) that contain three or more up- and down-steps. The remaining patches were not included, because they showed too few up- and down-steps, which did not allowed for a reliable estimate of the mean.

VI. Additional Methods

1. Synaptotagmin II knockout

Mice lacking Syt2 were described in detail earlier[15,16]. In short, they were generated by replacing part of exon 2 through exon 7 of the Syt2 gene with a *lacZ* DNA construct using homologous recombination[15]. Mutant mice were crossed into a C57BL/6 background. Mice for these experiments were obtained by heterozygous breeding using standard mouse husbandry procedures[15,16]. Genotyping was performed by PCR, which was previously confirmed to correlate with Syt2 expression by immunoblotting[15,16]. In some experiments, we confirmed that *Syt2*$^{-/-}$ mice did not show any antibody staining against Syt2 (Fig. S8) (see also Ref. [15]). As previously characterized[15], the EPSC in *Syt2*$^{-/-}$ mice was very small and less synchronized (e.g., Fig. 4e).

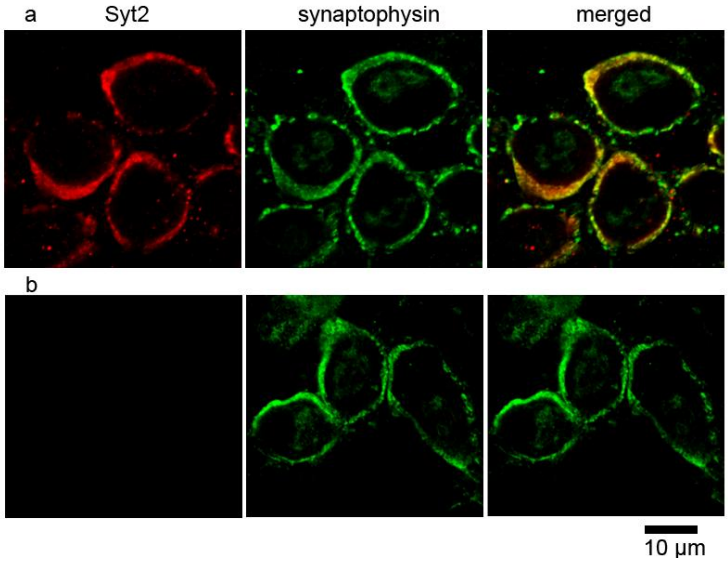

Figure S8. Syt2 immunostaining of calyx of Held

a, A tissue section double-labeled with antibodies against Syt2 (left, red) and synaptophysin (middle, green) revealed overlapping staining (right) in calyces of a *Syt2*$^{+/+}$ mouse.

b, Similar to panel a, but in a *Syt2*$^{-/-}$ mouse, revealing absence of Syt2.

2. Electron microscopy

For EM experiments, parasigittal brainstem slices (300 µm thick, only the middle 100 µm were used for examination) containing the medial nucleus of the trapezoid body were prepared. Slices were treated with 75 mM KCl for 1-2 min or control bath solution, and rapidly transferred to 0.1 N cacodylate buffer solution containing 2% glutaraldehyde and 2% paraformaldehyde (freshly prepared, Polyscience Europe GmbH, Eppelheim, Germany) for at least 1 hr at room temperature. The fixed slices were stored in 4°C refrigerator overnight. The next day, slices were washed with 0.1N cacodylate buffer before trimming.

Samples after trimming were treated with 1% OsO_4 in cacodylate buffer for 1 hr on ice, and 0.25% uranyl acetate in acetate buffer at pH 5.0 overnight at 4 °C, dehydrated with ethanol, and embedded in epoxy resin. Thin sections were counterstained with uranyl acetate and lead citrate.

Serial ultra-thin sections (~90 nm in thickness) through the MNTB were taken for measurements of the vesicle size. Photographs of these thin sections were collected with

a CCD digital camera system (XR-100 from AMT, Danvers, MA) at a primary magnification of 10,000-20,000X and saved in the zero loss file format (TIFF).

Measurements of vesicle diameter were made in the digital images on vesicles that showed clearly delineated membrane profiles indicating that they were likely fully embedded in the 90 nm section. Since the shape of some vesicles is slightly elliptical, diameters of vesicles were measured generally for perpendicularly oriented long (a_1) and short (b_1) axes between the outsides of the outer leaflets, and between the insides of the inner leaflets (a_2, b_2). The mean diameter (d) was approximated by $d=[(a_1*b_1*c_1)^{1/3} + (a_2*b_2*c_2)^{1/3}]/2$, where $c_1 = (a_1 + b_1)/2$, and $c_2 = (a_2 + b_2)/2$ (Ref. [17]). Some smaller vesicle profiles were likely resulted from sections of vesicles cut at less than their diameters. Some studies corrected this sectioning artifact by the equation $D = 2*[d - h + (d^2 + h^2 + dh\pi - 2dh)^{1/2}]/\pi$, where D is the corrected diameter, h is the section thickness[18]. We did not perform such correction because we did not find significant difference after correction.

Reference List

[1] Sudhof, T. C., The synaptic vesicle cycle, Annu. Rev. Neurosci **27**, 509-547 (2004).

[2] Wu, L. G., Ryan, T. A., & Lagnado, L., Modes of vesicle retrieval at ribbon synapses, calyx-type synapses, and small central synapses, J. Neurosci. **27**, 11793-11802 (2007).

[3] Singer, J. H., Lassova, L., Vardi, N., & Diamond, J. S., Coordinated multivesicular release at a mammalian ribbon synapse, Nat. Neurosci **7**, 826-833 (2004).

[4] Matthews, G. & Sterling, P., Evidence that vesicles undergo compound fusion on the synaptic ribbon, J. Neurosci. **28**, 5403-5411 (2008).

[5] He, L., Wu, X. S., Mohan, R., & Wu, L. G., Two modes of fusion pore opening revealed by cell-attached recordings at a synapse, Nature **444**, 102-105 (2006).

[6] Sätzler, K., *et al.*, Three-dimensional reconstruction of a calyx of Held and its postsynaptic principal neuron in the medial nucleus of the trapezoid body, J Neurosci **22**, 10567-10579 (2002).

[7] J. R. Stiles, *et al.*, "Synaptic Variability,"in *Synapses,* edited by T. C. Cowan, T. C. Sudhof, and C. F. Stevens (The Johns Hopkins University Press, Baltimore, 2000), pp.681-732.

[8] Nielsen, T. A., Digregorio, D. A., & Silver, R. A., Modulation of glutamate mobility reveals the mechanism underlying slow-rising AMPAR EPSCs and the diffusion coefficient in the synaptic cleft, Neuron **42**, 757-771 (2004).

[9] Stiles, J. R., Van Helden, D., Bartol, T. M., Jr., Salpeter, E. E., & Salpeter, M. M., Miniature endplate current rise times less than 100 microseconds from improved dual recordings can be modeled with passive acetylcholine diffusion from a synaptic vesicle, Proc. Natl. Acad. Sci. U. S. A **93**, 5747-5752 (1996).

[10] Hausser, M. & Roth, A., Dendritic and somatic glutamate receptor channels in rat cerebellar Purkinje cells, J Physiol **501 (Pt 1)**, 77-95 (1997).

[11] Spruce, A. E., Breckenridge, L. J., Lee, A. K., & Almers, W., Properties of the fusion pore that forms during exocytosis of a mast cell secretory vesicle, Neuron **4**, 643-654 (1990).

[12] Sahara, Y. & Takahashi, T., Quantal components of the excitatory postsynaptic currents at a rat central auditory synapse, J Physiol **536**, 189-197 (2001).

[13] Wu, X. S., *et al.*, The origin of quantal size variation: vesicular glutamate concentration plays a significant role, J Neurosci **27**, 3046-3056 (2007).

[14] Ishikawa, T., Sahara, Y., & Takahashi, T., A single packet of transmitter does not saturate postsynaptic glutamate receptors, Neuron **34**, 613-621 (2002).

[15] Sun, J., *et al.*, A dual-Ca2+-sensor model for neurotransmitter release in a central synapse, Nature **450**, 676-682 (2007).

[16] Pang, Z. P., *et al.*, Synaptotagmin-2 is essential for survival and contributes to Ca2+ triggering of neurotransmitter release in central and neuromuscular synapses, J. Neurosci. **26**, 13493-13504 (2006).

[17] Bruns, D., Riedel, D., Klingauf, J., & Jahn, R., Quantal release of serotonin, Neuron **28**, 205-220 (2000).

[18] Parsons, T. D., Coorssen, J. R., Horstmann, H., & Almers, W., Docked granules, the exocytic burst, and the need for ATP hydrolysis in endocrine cells, Neuron **15**, 1085-1096 (1995).